NeuroImage 231 (2021) 117832

Contents lists available at ScienceDirect

NeuroImage

journal homepage: www.elsevier.com/locate/neuroimage

Vascular risk factors are associated with a decline in resting-state functional connectivity in cognitively unimpaired individuals at risk for Alzheimer's disease ☆
Vascular risk factors and functional connectivity changes

Theresa Köbe[a,b,c,*], Alexa Pichet Binette[a,b], Jacob W. Vogel[d], Pierre-François Meyer[a,b], John C.S. Breitner[a,b], Judes Poirier[a,b], Sylvia Villeneuve[a,b,e,**], for the Presymptomatic Evaluation of Novel or Experimental Treatments for Alzheimer Disease (PREVENT-AD) Research Group

[a] Department of Psychiatry, McGill University, H3A 1A1, Montreal, Quebec, Canada
[b] Douglas Mental Health University Institute, Studies on Prevention of Alzheimer's Disease (StoP-AD) Centre, H4H 1R3, Montreal, Quebec, Canada
[c] German Center for Neurodegenerative Diseases (DZNE), 01307, Dresden, Germany
[d] Montreal Neurological Institute, McGill University, H3A 2B4, Montreal, QC, Canada
[e] Department of Neurology and Neurosurgery, McGill University, H3A 2B4, Montreal, Quebec, Canada

ARTICLE INFO

Keywords:
β-Amyloid
Global functional connectivity
Default-mode network
Longitudinal resting-state functional connectivity
tau
Vascular risk factors

ABSTRACT

Resting-state functional connectivity is suggested to be cross-sectionally associated with both vascular burden and Alzheimer's disease (AD) pathology. However, evidence is lacking regarding longitudinal changes in functional connectivity. This study includes 247 cognitively unimpaired individuals with a family history of sporadic AD (185 women/ 62 men; mean [SD] age of 63 [5.3] years). Plasma total-, HDL-, and LDL-cholesterol and systolic and diastolic blood pressure were measured at baseline. Global (whole-brain) brain functional connectivity and connectivity from canonical functional networks were computed from resting-state functional MRI obtained at baseline and ~3.5 years of annual follow-ups, using a predefined functional parcellation. A subsample underwent A*β*- and *tau*-PET (n=91). Linear mixed-effects models demonstrated that global functional connectivity increased over time across the entire sample. In contrast, higher total-cholesterol and LDL-cholesterol levels were associated with greater reduction of functional connectivity in the default-mode network over time. In addition, higher diastolic blood pressure was associated with global functional connectivity reduction. The associations were similar when the analyses were repeated using two other functional brain parcellations. A*β* and *tau* deposition in the brain were not associated with changes in functional connectivity over time in the subsample. These findings provide evidence that vascular burden is associated with a decrease in functional connectivity over time in older adults with elevated risk for AD. Future studies are needed to determine if the impact of vascular risk factors on functional brain changes precede the impact of AD pathology on functional brain changes.

1. Introduction

Both aging and Alzheimer's disease (AD) are characterized by early vascular dysfunctions (Kannel et al., 2009; Iturria-Medina et al., 2016) and changes in brain functional connectivity (Betzel et al., 2014; Hohenfeld et al., 2018). AD is additionally characterized by pathological protein aggregations in the brain (amyloid-*β* (A*β*) and *tau*) (Small et al., 2008). Vascular risk factors (VRFs) such as dyslipidemia, diabetes and hypertension are thought to impair healthy aging and to increase AD risk (Zlokovic, 2011; Köbe et al., 2020) via several pathways including functional brain disruptions and AD pathology (Rodrigue et al., 2013; Iturria-Medina et al., 2016). An association between VRFs and A*β*, but

☆ Data used in preparation for this article were obtained from the Pre-symptomatic Evaluation of Novel or Experimental Treatments for Alzheimer's Disease (PREVENT-AD) program (https://douglas.research.mcgill.ca/stop-ad-centre), data release 5.0 (November 30, 2017).

** Corresponding author at: Department of Psychiatry, McGill University, Faculty of Medicine, Douglas Mental Health University Institute, Perry Pavilion, Room E3417.1, 6875 LaSalle Blvd, Montreal, QC H4H 1R3, Canada
* Corresponding author.
E-mail addresses: theresa.koebe@dzne.de (T. Köbe), sylvia.villeneuve@mcgill.ca (S. Villeneuve).

https://doi.org/10.1016/j.neuroimage.2021.117832
Received 30 October 2020; Received in revised form 25 January 2021; Accepted 27 January 2021
Available online 4 February 2021

not tau, was previously reported in 75 participants free from vascular medication included in a previous study (Köbe et al., 2020). Brain regions that show a temporal correlation in blood-oxygenation-level-dependent (BOLD) signals, measured with resting-state functional magnetic resonance imaging (rs-fMRI), have been proposed to be intrinsically functionally connected. Consistent resting-state functional connectivity (RSFC) networks have been identified in a large number of studies using different brain parcellations (Power et al., 2011; Schaefer et al., 2018; Urchs et al., 2019).

With age, RSFC appears to decline within most networks while increasing between networks (Betzel et al., 2014). In fact, it has recently been suggested that global and default-mode network (DMN) RSFC tend to increase up to the seventh decade, followed thereafter by an accelerated age-related decline (Staffaroni et al., 2018). Similar alterations in RSFC have also been consistently linked to mild cognitive impairment and AD dementia, particularly with lower RSFC in the DMN, but also in the salience (SAL) and limbic (LIM) networks and changes in global RSFC (Brier et al., 2012; Myers et al., 2014; Tam et al., 2015; Jones et al., 2016; Badhwar et al., 2017; Mutlu et al., 2017). AD-related alterations in RSFC are already present in the asymptomatic stage, years before disease onset (Hedden et al., 2009; Elman et al., 2016). In this early disease stage functional changes associated with AD risk are not only linked to a reduction of RSFC, but also to a compensatory increase in RSFC (Elman et al., 2016; Verfaillie et al., 2018). The extent to which these RSFC alterations in aging and preclinical AD are related to VRFs still needs to be better understood. Furthermore, while VRFs are often studied by computing an aggregate burden score, hypertension and hypercholesterolemia might impair brain integrity via different mechanisms that reinforce each other (Carmichael, 2014).

Cross-sectional studies have shown that higher vascular burden is associated with reduced cerebral metabolism, reduced cerebrovascular reactivity and an associated reduction in functional connectivity (Liu, 2013; Haight et al., 2015; Rashid et al., 2019; Zonneveld et al., 2019). While elevated blood pressure is believed to promote arterial stiffness, leading both to increased mechanical stress and less efficient oxygen transfer to smaller cerebral blood vessels, higher cholesterol levels seem to promote the formation of atherosclerotic plaques, causing altered dynamics in blood flow through stenotic cerebral blood vessels (Carmichael, 2014). Hypertension has been suggested to impair frontoparietal networks in older adults (Li et al., 2015) while higher total-cholesterol levels have been associated with both lower and higher RSFC within the DMN and lower RSFC within the SAL network (Xia et al., 2015; Zhang et al., 2016). So far, whether blood pressure and/or cholesterol levels show associations with changes in brain functional connectivity over time, and if so which network(s) show these associations, remain open questions. According to the two-hit vascular hypothesis of AD (Zlokovic, 2011), VRFs first reduce brain functional health and increase vulnerability to cascading events that precede dementia, before Aβ and *tau* pathologies affect brain integrity as a second hit, leading to cognitive impairment.

In the current study, we aimed to investigate how RSFC alterations develop over time in the presence of VRFs and early AD biomarkers. We applied longitudinal rs-fMRI to delineate related changes in functional connectivity in cognitively normal individuals who had a 2-3 fold higher risk for AD owing to a first-degree family history of the disease (Goldman et al., 2011). Our main hypothesis was that individuals with higher VRFs would show a decrease in RSFC over time, and that this reduction would be predominant in the DMN for individuals with higher cholesterol levels and in the frontoparietal network for individuals with higher blood pressure. Second, we hypothesized that the presence of higher Aβ and *tau* burden will result in similar connectivity changes, with Aβ being predominantly associated with a change in the DMN and *tau* with a change in the limbic network. Both pathologies accumulate first within these respective brain networks in the AD process (Palmqvist et al., 2017; Vogel et al., 2020).

2. Materials and methods

2.1. Participants and Study design

Study participants were recruited within the *PResymptomatic EValuation of Experimental or Novel Treatments for Alzheimer Disease* (PREVENT-AD) study, an ongoing longitudinal observational study initially enrolling 385 individuals (Breitner et al., 2016). Most of this dataset is now openly accessible (https://registeredpreventad.loris.ca/). Study participants met the following inclusion criteria: (a) parental or multiple-sibling history of AD-like dementia, (b) ≥60 years old at enrollment or 55–59 years old if less than 15 years away from the youngest affected relative's age of symptom onset, (c) no major neurological diseases and (d) normal cognition. All participants underwent a short neuropsychological screening at study entry, using Clinical Dementia Rating (CDR) (Morris, 1993) and Montreal Cognitive Assessment (MOCA) (Nasreddine et al., 2005) to assess normal cognition. In a few cases of ambiguous CDR or MOCA assessments (n=15, MOCA ≤ 26/30 or CDR = 0.5), participants were further evaluated with a more extensive neuropsychological battery, including the Repeatable Battery for the Assessment of Neuropsychological Status (RBANS) (Randolph et al., 1998) which was reviewed by certified neuropsychologists (including SV) and physicians (including JCSB) to ensure normal cognition. In total, 15 study participants (6%) converted to MCI patients after the first (n=1), second (n=3), third (n=5) and fourth (n=6) year of follow-up (all rs-fMRI time points were retained in the analyses). **Fig. 1** provides an overview of the study.

In the current longitudinal analyses, 247 participants who had at least 2 valid fMRI scans were included.

2.2. Standard protocol approvals, registrations, and patient consents

The study was approved by the McGill University Faculty of Medicine Institutional Review Board. All participants received detailed study instructions and gave written consent prior to participation.

2.3. VRF assessment

All participants were examined medically: venous blood samples (non-fasting) and blood pressure were taken at baseline, also described previously (Köbe et al., 2020). Plasma levels of total-, high-density (HDL)- and low-density lipoprotein (LDL)-cholesterol were measured by standard enzymatic methods (CHOD-PAP; Beckman Coulter, Synchron LX®, UniCel® DxC 600/800 System and Synchron® Systems Lipid Calibrator). Blood pressure was assessed while seated in a standardized procedure using an automatic sphygmomanometer (Connex® ProBP™ 3400; Welch Allyn). All venous blood samples were taken non-fasting; because most of an individual's lifetime is spent in the postprandial state (Rifai et al., 2016), lipid profiles change minimally in response to normal food intake, and non-fasting lipid profiles seem to predict increased risk of cardiovascular events better than fasting lipid profiles (Fatima et al., 2016; Langsted et al., 2019).

2.4. *APOE* genotyping

Genomic DNA was extracted from whole blood and *APOE* genotype was determined using the PyroMark Q96 pyrosequencer (Qiagen, Toronto, ON, Canada) and the following primers: rs429358_amplification_forward 5′-ACGGCTGTCCAAGGAGCTG-3′, rs429358_amplification_reverse_biotinylated 5′-CACCTCGCCGCGGTACTG-3′, rs429358_sequencing 5′-CGGACATGGAGGACG-3′, rs7412_amplification_forward 5′-CTCCGCGATGCCGATGAC-3′, rs7412_amplification_reverse_biotinylated 5′-CCCCGGCCTGGTACACTG-3′ and rs7412_sequencing 5'-CGATGACCTGCAGAAG-3'; also described previously (Meyer et al.,

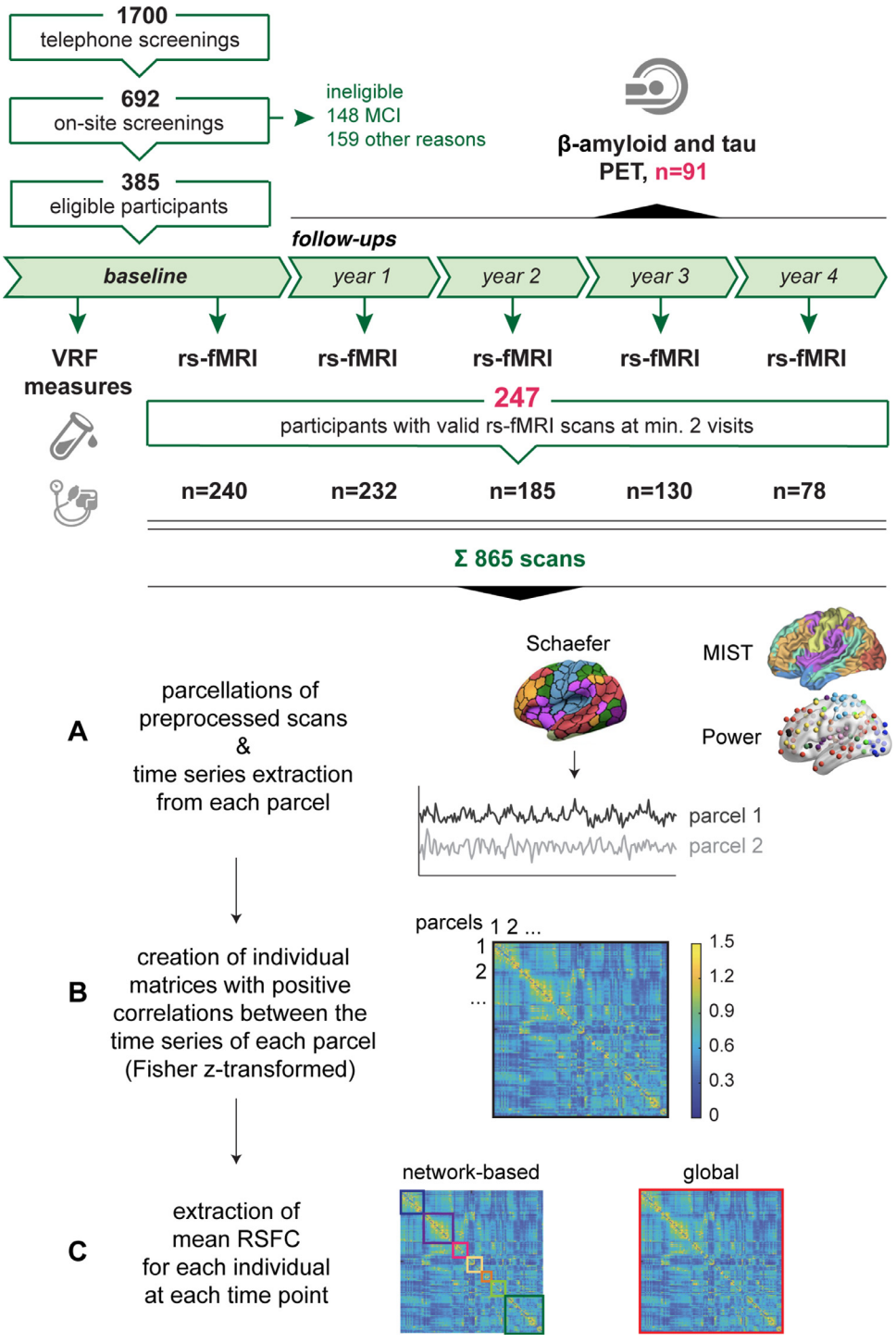

Fig. 1. *Study flow chart and fMRI analyses.* In total, 385 eligible PREVENT-AD participants were followed annually over up to 4 years. Vascular risk factors were assessed at baseline. Resting-state functional magnetic resonance images (rs-fMRI) were acquired at baseline and follow-up year 1 to 4. Finally, 247 participants with 865 scans were included in the current study, who had at least 2 valid rs-fMRI scans across baseline (n=240 scans), follow-up year 1 (n=232), year 2 (n=185), year 3 (n=130) and year 4 (n=78). For 7 participants the first valid MRI scan was available at follow-up year 1 (n=5) and 2 (n=2) instead of at baseline. (A) Individual time series of preprocessed scans were extracted from each parcel, defined by the Schaefer parcellations. Analyses were repeated with the MIST and Power atlas. (B) Correlation matrices were obtained by correlating the time series of each parcel with one another. Correlation matrices were Fisher z-transformed and thresholded by only keeping positive correlations. (C) Extracted mean correlations represent the indirect measure of network-based (multicolored squares) and global (red square) resting-state functional connectivity (RSFC). A subsample of 91 participants that had two rs-fMRI scans underwent Aβ and tau PET scanning during the course of the study.

2018). Participants were classified as *APOE* ε4 carriers (one or two ε4 alleles) or noncarriers.

2.5. MRI acquisition

Participants underwent MRI annually (at baseline and at follow-ups from 1 to 4 years) on a 3T Siemens Trio scanner at the Brain Imaging Centre of the Douglas Mental Health University Institute (Montreal, Canada). Structural T1-weighted images were obtained with the following parameters: TR = 2300ms, TE = 2.98 ms, number of slices=176, slice thickness=1 mm. For resting-state functional MRI (rs-fMRI) scans, two consecutive functional T2*-weighted images (each "run" with 150 volumes lasting 5 min and 45 s) were acquired using a blood-oxygen-level-dependent (BOLD) sensitive, single-shot echo planar sequence (TR=2000 ms; volumes=150; TE=30 ms; FA = 90°; matrix size=64 × 64; voxel size=4 × 4 × 4 mm^3; 32 slices). The participants were asked to keep their eyes closed and to remain as still as possible during scanning.

2.6. MRI analyses

Preprocessing and analyses of the rs-fMRI data has been described previously (Verfaillie et al., 2018), using the Neuroimaging Analysis Kit (http://niak.simexp-lab.org, v0.12.17), GNU Octave (v4.0), and the Minc toolkit (http://www.bic.mni.mcgill.ca/ServicesSoftware/

Table 1
Overview MRI flow.

Numbers of:	BL	FU year 1	FU year 2	FU year 3	FU year 4	Total
acquired MRI scans	363	294	232	169	94	1152
failed quality control	−51	−51	−43	−37	−16	−198
(reason [a]/[b]/[c])	(50[a]/1[b])	(48[a]/3[c])	(42[a]/1[c])	(37[a])	(16[a])	(193[a]/1[b]/4[c])
valid MRI scans	312	243	189	132	78	954
number of individuals	240	232	185	130	78	865
with at least 2 valid MRI scans (with one/ two runs)	(20/220)	(17/215)	(28/157)	(13/117)	(12/66)	(90/775) = 247 unique individuals
average number of valid MRI frames (max. 150)	130	126	126	125	124	

Reasons for failure of quality control.
[a] <70 unscrubbed frames per run
[b] image artefacts
[c] registration failure. For 7 participants the first valid resting-state fMRI scans were available at follow-up year 1 (n=5) and year 2 (n=2) instead at baseline, but all participants needed to have at least two time points with a valid fMRI scan. BL, baseline; FU, follow-up.

ServicesSoftwareMinc ToolKit, v0.3.18). Briefly, the preprocessing of functional scans comprised motion-correction, slice-time correction, temporal filtering (0.01 Hz high-pass cut-off), non-linear spatially normalization to the Montreal Neurological Institute ICBM152 symmetric template, resampling to 2 mm^3, and spatial smoothing with a 6mm full-width-half-maximum (FWHM) Gaussian kernel. Noise due to motion, slow time drifts, and average signals in white matter and the lateral ventricles was removed from the functional signal by multiple regression (http://niak.simexplab.org/pipe_preprocessing.html) (Orban et al., 2015; Verfaillie et al., 2018). Global signal regression was not performed. In addition, time frames with in-scanner head motion (mean framewise displacement (FD)) above 0.5mm were removed (scrubbed) from individual time series, along with one adjacent frame prior and two following frames after, to minimize artefacts caused by excessive motion (Power et al., 2012). Mean FD was calculated after scrubbing to be used as a covariate in the statistical analyses. Further descriptions of the pipeline can be found on the NIAK website (http://niak.simexplab.org/build/html/PREPROCESSING.html). Moreover, rs-fMRI images passed quality control if: (a) at least one out of two functional runs remained with a minimum of 70 frames (140s) after scrubbing; (b) no image artefacts were found during visual examination; (c) they were correctly co-registered to structural MRI and ICBM152 template (spatial correlation r>0.75, NIAK preprocessing report). At least 75% of our study sample showed a minimum of 108 valid frames at each time point, indicating a high data quality.

In total, 1152 rs-fMRI scans were acquired within the PREVENT-AD cohort at 5 acquisition time points (baseline and follow-ups at year 1 to 4), of which 198 scans failed quality control, leaving 954 valid scans. For the current longitudinal analyses, participants were required to have at least 2 valid scans at different time points, resulting in 865 scans from 247 individuals (median [interquartile range] number of scans, 4 [2-4] and follow-up time, 3 [2-4] years) (see **Table 1**).

For *a priori* network-based and global connectivity analyses, we used the "Schaefer parcellation" (Schaefer et al., 2018). This parcellation scheme includes 400 predefined parcels classified into 7 neocortical functional networks (default mode [DMN], salience and ventral attention [SAL/VAN], fronto-parietal [FPN], limbic [LIM], dorsal attention [DAN], visual [VIS] and somatomotor network [SM]). To ensure the robustness of our findings, we repeated our analyses using 2 different predefined parcellation schemes. The second parcellation was the "MIST parcellation" (Urchs et al., 2019), consisting of 444 symmetric parcels that belong to 7 functional networks (DMN, SAL/VAN, FPN, LIM, VIS, SM and cerebellum). We restricted the analyses to neocortical functional networks to match the Schaefer parcellation and therefore excluded the cerebellum. The third atlas was the "Power parcellation", including 264 parcels made up of 5mm radius spheres (Vachon-Presseau et al., 2019) set around network coordinates predefined by Power et al. (Power et al., 2011); thus, varying in shape and number from the other two parcellation schemes. Here, we restricted our network analyses to the 7 matching neocortical functional networks, i.e. DMN, SAL, VAN, FPN, DAN, VIS and SM, and included 8 additional spherical parcels (5mm radius) encompassing the LIM as done previously (Vachon-Presseau et al., 2019).

For each atlas, the average time series from each parcel was extracted, correlated with one another (Pearson) and Fisher z-transformed, using Matlab (R2018b). Hence, single-subject correlation matrices were created (400 × 400, 444 × 444 and 272 × 272 for the Schaefer, MIST and Power parcellation, respectively). For participants who had 2 valid rs-fMRI runs per visit, correlation matrices were averaged after processing. Results were essentially unchanged when correcting our subsequent statistical models for the number of valid runs (1 or 2) at each visit. Given the ambiguous interpretation of negative correlations, correlation matrices were thresholded to keep only positive correlations (Murphy et al., 2009). Density of individual correlation matrices (no. of positive correlations/no. of possible correlations) was consistent across all time points both when looking at the whole matrix or within networks (on average 72-91% connections were retained; **Supplemental Table S1**). Finally, correlation estimates from parcels of the same network were averaged, providing a mean RSFC within each functional network. In addition, we computed the global (whole-brain) RSFC for each participant, corresponding to the average connectivity of each parcel to the entire rest of the cerebrum (Schaefer: 400 × 400; MIST: 387 × 387 (cerebellum parcels excluded); and Power: 232 × 232 (cerebellum and as uncertain defined parcels excluded)). We investigated both network-specific and global functional connectivity given that specific and global brain connections seem to be differentially associated to brain alterations and AD-related biomarkers (Mutlu et al., 2017). An overview of the rs-fMRI processing and analyses is represented in **Fig. 1**.

2.7. PET assessment and processing

In a subsample of 91 (37%) participants, PET scans (amyloid-β, [^{18}F]NAV4694 (NAV) provided by Navidea Biopharmaceuticals (Dublin, Ohio) and *tau*, [^{18}F]AV1451 (Flortaucipir) provided by Eli Lilly & Company (Indianapolis, Indiana)) were acquired ordinarily on two consecutive days during the course of the study at the McConnell Brain Imaging Centre of the Montreal Neurological Institute (MNI) on a PET Siemens/CTI high-resolution scanner (Köbe et al., 2020). Approximately 6 mCi of NAV and 10 mCi of Flortaucipir were injected intravenously. Static acquisition frames were obtained for Aβ at 40-70 min (6 × 5 min frames) and for *tau* at 80–100 min (4 × 5 min frames) post-injection. PET data were pre-processed using a standard pipeline (see https://github.com/villeneuvelab/vlpp for details). Briefly, 4D PET

images were averaged and linearly co-registered to individual's T1-weighted images, before being masked to exclude CSF binding and smoothed with a 6mm^3 Gaussian kernel. Individual T1-weighted images were segmented based on the Desikan-Killiany atlas using the semi-automated FreeSurfer processing stream version 5.3 (Desikan et al., 2006). Standardized uptake value ratios (SUVR) were computed for Aβ (Villeneuve et al., 2015) and *tau* (Baker et al., 2017) by dividing the tracer uptake by cerebellar gray matter and inferior cerebellar gray matter uptake, respectively. We restricted the analyses to FreeSurfer-derived typical AD regions, i.e. weighted mean SUVRs from frontal, temporal, parietal and posterior cingulate cortex for a global Aβ quantification (Villeneuve et al., 2015; McSweeney et al., 2020) and from the entorhinal cortex for *tau* quantification (Schöll et al., 2016).

2.8. Statistical analyses

Analyses were performed with R 3.5.2 (The R Foundation) and SPSS 24.0 (IBM Corp., Armonk, NY). Two-tailed *p*-values <0.05 were considered to be significant.

First, we ran cross-sectional general linear models (GLM) to test for associations between VRFs and network/global RSFC at baseline, corrected for baseline age, sex, vascular medication (intake or non-intake of drugs to treat dyslipidemia and/or hypertension) and mean FD.

Second, we performed linear mixed-effects models (LME, lmer function of the *lme4* package (Bates et al., 2015)), including time as independent variable and age, sex and mean FD as covariates to characterize the overall change in network/global RSFC over time in the entire cohort. Follow-up time was operationalized individually as years from baseline.

Variability of global and network RSFC was assessed by calculating the coefficients of variation (CV; standard deviation/mean of RSFC) at each time point. We used the modified signed-likelihood ratio (MSLR) test from the R software package "cvequality" version 0.2.0 (Marwick et al., 2019) to test for significant differences in the CVs of network-based and global RSFC between time points.

Third, we ran LME models including baseline cholesterol and blood pressure measures to test if longitudinal changes in RSFC vary in relation to these VRFs. All the VRF measures were entered in the same statistical model, but because total- and LDL-cholesterol exhibit a high multicollinearity (variance inflation factor > 5: total-cholesterol ~9 and LDL-cholesterol ~8), we first ran a model with total-cholesterol that excluded LDL-cholesterol and then repeated this model, replacing total-cholesterol by LDL-cholesterol. The results related to HDL-cholesterol, systolic blood pressure and diastolic blood pressure were highly similar in both models. Thus, for simplicity, results from the models which included total-cholesterol are reported in the main manuscript and results from the models which included LDL-cholesterol are reported in supplementary material. Baseline age, sex, vascular medication and mean FD at each visit were included as potential confounding factors. Models included all main effects as well as their interactions with time. Finally, we tested the impact of *APOE* ε4 on these associations between VRF and longitudinal RSFC change and for an association between *APOE* ε4 and changes in RSFC over time while correcting for age, sex and mean FD.

In a subgroup of individuals with PET scans (n=91), we tested for an association of Aβ and *tau* deposition with RSFC at baseline using GMLs, and with changes in RSFC over time using LME models corrected for age, sex and mean FD as well as their interactions with time. Here, the RSFC time variable was centered on the PET visit for each individual since the PET scans were acquired during the course of the study.

In all LME models, we included next to the fixed effects (variables of interest (i.e., VRFs) and covariates (age, sex, etc.)), individual RSFC intercepts and slopes as random effects. All continuous variables were z-transformed prior to model estimation. All models used the restricted maximum likelihood method and were fit with an unstructured variance-covariance and type III sum of squares. Denominator degrees of freedom were calculated with the Satterthwaite approximations. An overview of the LME models is provided in the **Supplementary material**. For each research question, results from each LME network model were jointly evaluated per parcellation for significance at a False Discovery Rate (FDR) corrected *p*-values <0.05. Uncorrected p-values were reported in the manuscript and when results survived FDR correction, this was explicitly stated.

3. Results

3.1. Participant characteristics

A total of 247 participants was included in the current longitudinal analyses. At study entry, they were on average 63 years old, had a mean education of 15.4 years, and 75% were female. The percentage of participants carrying at least one *APOE* ε4 allele was 39%, which is above the average ε4 allele frequency within the general population of cognitively unimpaired older adults (~23–32%) (McKay et al., 2011). This may underline the increased risk of the Prevent-AD cohort for late-onset AD. Participants were on average 11 years away from their relative's age at AD dementia symptom onset. The subgroup of 91 participants with PET showed low to moderate levels of Aβ and *tau* deposition (see **Table 2** for further details). Participants were generally in good health. Abnormal levels of VRFs were predominantly recorded for total-cholesterol levels (>5.2 mmol/L; 63% of the participants), LDL-cholesterol (>3.4 mmol/L; 38%), systolic blood pressure (≥130 mmHg; 43%), diastolic blood pressure (≥80 mmHg; 29%) and body mass index (>30 kg/m^2; 14%). About 4% of the study sample was diagnosed with diabetes and 4% of the participants reported current smoking.

3.2. Impact of VRFs on baseline RSFC

At baseline, we found no associations between VRFs and network or global functional connectivity (all *p*'s≥0.05). Higher HDL-cholesterol levels were associated with lower baseline RSFC within the DMN (Schaefer parcellation) and DAN network (Power parcellation), but these associations were driven by two outlier cases (±2 standard deviations of mean RSFC, see **Supplemental Table S2 and Supplemental Figure S1)**.

3.3. Global and network specific longitudinal change in RSFC across all individuals

In the entire cohort, we found an overall increase in global RSFC over time when adjusted for age, sex and mean FD (Schaefer: β=0.009, s.e.=0.003, t=2.97, p=0.003; black dotted lines in Fig. 3). Similar results were obtained when using the MIST and Power parcellation (MIST: β=0.009, s.e.=0.003, t=3.00, p=0.003; Power: β=0.010, s.e.=0.002, t=2.48, p=0.014; **Supplemental Figure S3**). No changes in DMN RSFC were observed over time using any of the 3 parcellations (all *p*'s≥0.05). An overall increase in RSFC was found within specific functional networks across all individuals (Schaefer: in LIM and DAN, β's ≥0.016, s.e.'s ≤0.006, t's ≥2.97 *p*'s <0.003; MIST: in FPN and LIM, β's ≥0.010, s.e.'s ≤0.004, t's ≥2.09 *p*'s ≤0.037; Power: in DAN and SM, β's ≥0.011, s.e.'s ≤0.007, *t*'s ≥2.05 *p*'s ≤0.040; **Supplemental Figure S3**). Regarding variability in connectivity, no significant differences in CV of network-based or global RSFC were found between the timepoints (all MSLR tests ≤ 8.3, $p \geq 0.080$; see variability of RSFC measures across time points in **Supplemental Figure S4**).

3.4. Impact of VRFs on longitudinal change in RSFC

Investigating how longitudinal changes in RSFC are related to VRFs, we found no associations between any of the cholesterol values and global connectivity changes over time (**Figs. 2** and **3, Supplemental Table S3**). However, higher total-cholesterol levels were associated with decreased RSFC within the DMN (Schaefer, β=-0.013, s.e.=0.004, t=-3.26, p=0.001; **Figs. 2** and **3, Supplemental Table S3**). This association survived FDR-correction and was similar when using the MIST

Table 2
Participant characteristics at baseline.

Characteristics	Mean (SD; range)
Sample size [No.]	247
Age [years]	62.90 (5.31; 55–83)
Sex [No. women (%)]	185 (75)
Education [years]	15.37 (3.58; 7–29)
APOE ε4 [No. carrier, ≥1 ε4 allele (%)]	96 (39)
spEYO [years][a]	-10.93 (7.58; -28–16)
Plasma lipids [mmol/L]	
Total-cholesterol	5.48 (0.99; 2.20–8.30)
HDL-cholesterol	1.57 (0.40; 0.74–3.04)
LDL-cholesterol[b]	3.09 (0.85; 0.78–5.77)
Arterial blood pressure [mm Hg]	
Systolic blood pressure	127.50 (15.87; 82–174)
Diastolic blood pressure	73.46 (9.17; 51–110)
Medication [No. (%)]	80 (32.4)
Lipid-lowering drugs	24 (9.7)
Antihypertensive drugs	32 (13.0)
Lipid-lowering & antihypertensive drugs	24 (9.7)
AD PET biomarkers [c]	
Aβ, [^{18}F]NAV-4694 SUVR [median (IQR), [range], % of Aβ positive individuals [d]]	1.21 (1.14-1.29), [1.05-2.81], 14.3
tau, [^{18}F]AV-1451 SUVR [median (IQR), [range]]	1.04 (0.98-1.14), [0.84-1.66]
Mean FD [e] (BL, FU1, FU2, FU3, FU4)	0.22 (0.05; 0.09–0.33) 0.22 (0.05; 0.09–0.35) 0.23 (0.05; 0.12–0.34) 0.23 (0.04; 0.10–0.33) 0.23 (0.05; 0.11–0.34)

[a] The spEYO could not be calculated for 16 participants due to missing information about the family's age of onset.
[b] LDL-cholesterol values were missing for 7 participants due to laboratory measurement failures.
[c] A subsample of 91 participants underwent β-amyloid (Aβ) and *tau* PET scanning during the course of the study. A previously estimated global Aβ positivity threshold of 1.37 was used to define Aβ+ individuals (McSweeney et al., 2020).
[e] The sample size of the fMRI data differs between BL (n=240), FU year 1 (n=232), FU year 2 (n=185); FU year 3 (n=130); FU year 4 (n=78). APOE ε4, apolipoprotein E ε4; BL, baseline; FD, framewise displacement; FU, follow-up; EYO, estimated years to symptom onset of sporadic Alzheimer's disease, calculated by subtracting the age at family's symptom onset from the participant's age at baseline.

and Power brain parcellations (**Supplemental Figures S2** and **S3, Supplemental Tables S4** and **S5**). Higher total-cholesterol was also related to a reduction in RSFC within the SAL network; however, this was only seen with the Power parcellation atlas (**Supplemental Figures S2** and **S3, Supplemental Table S5**). No longitudinal effects on RSFC were found for HDL-cholesterol. Substituting total-cholesterol for LDL, we found that higher LDL-cholesterol levels were associated with a decline in DMN RSFC (Schaefer, β=−0.010, s.e.=0.004, t=−2.30, p=0.023; **Figs. 2** and **3, Supplemental Table S3**). This was also shown with the MIST parcellation, and at trend-level with the Power parcellation (**Supplemental Figures S2** and **S3, Supplemental Tables S4** and S5).

In regard to blood pressure, higher diastolic blood pressure levels were associated with a reduction of global RSFC over time (Schaefer; β=−0.008, s.e.=0.004, t=−2.18, p=0.030; **Figs. 2** and **3, Supplemental Table S3**). This association was similar when using the MIST and Power brain parcellations (**Supplemental Figures S2** and **S3, Supplemental Tables S4** and **S5**). At the network level, associations were also found between higher diastolic blood pressure and reduction in RSFC within the DMN (Schaefer, β=−0.008, s.e.=0.004, t=−2.00, p=0.047), SAL/VAN (Schaefer, β=−0.010, s.e.=0.005, t=−1.98, p=0.049) and SM networks (Schaefer, β=−0.016, s.e.=0.008, t=-2.00, p=0.047) (**Fig. 2, Supplemental Figure S3** and **Supplemental Table S3**). No associations were found between systolic blood pressure and change in RSFC. All detailed statistical results can be found in **Supplemental Tables S3, S4 and S5**. Removing outliers (±2 standard deviations) of mean RSFC did not affect our findings of the associations of cholesterol and diastolic blood pressure with change in RSFC.

These results remained significant when controlling for *APOE* ε4 status and we did not find any associations between *APOE* ε4 allele status and changes in global or network-based functional connectivity over time (*APOE* ε4 × time interaction, all p's > 0.05, data not shown).

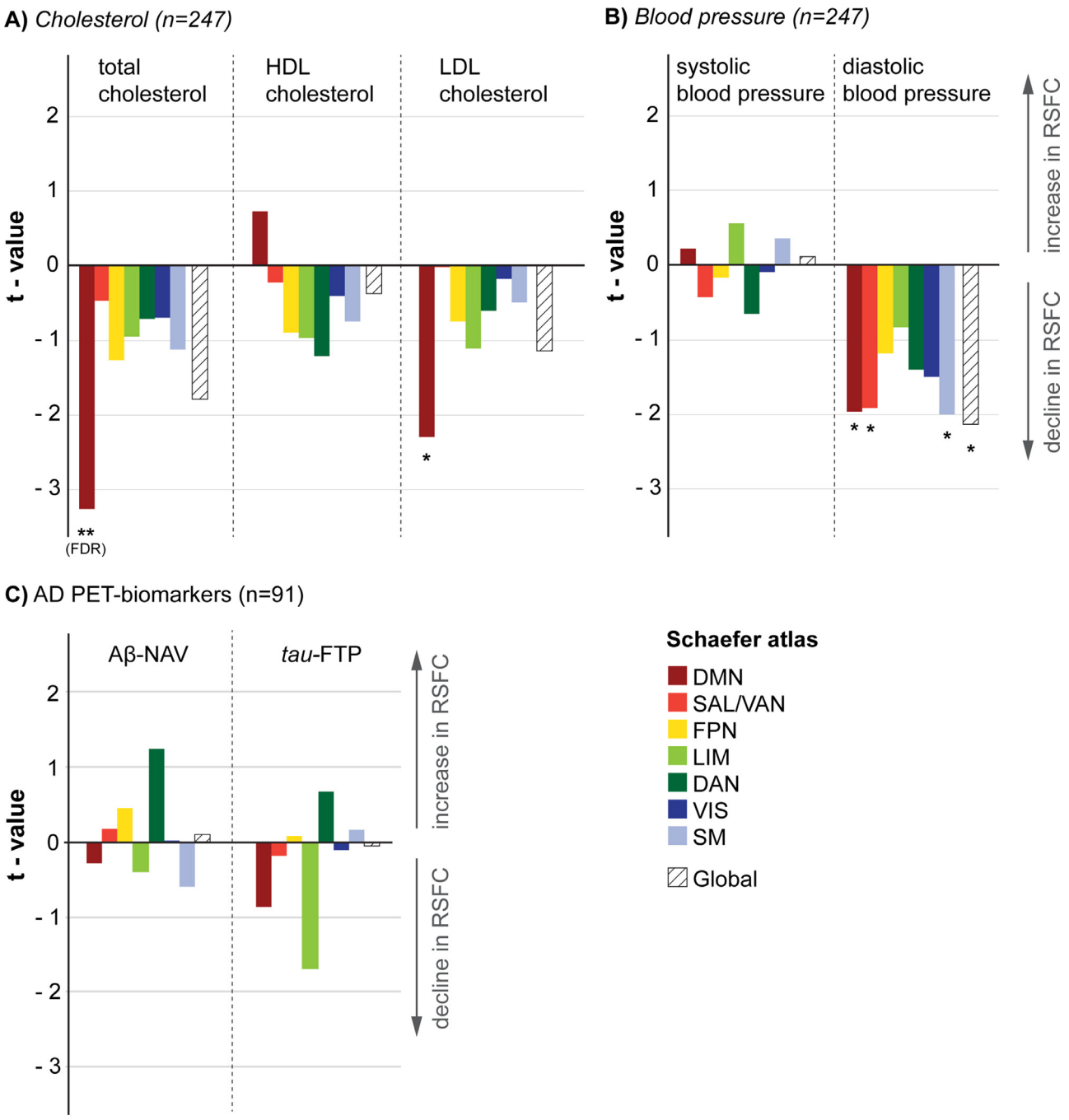

Fig. 2. *Summary of associations of VRF and AD biomarkers with changes in functional connectivity over time from linear mixed-effects models (see Supplemental Tables S3 and S6 for statistical summary tables).* T-values represent effects of (A) total-, HDL- and LDL-cholesterol, (B) systolic and diastolic blood pressure as well as (C) *β*-amyloid-(A*β*) and *tau*-PET SUVR on changes in each RSFC network and on global RSFC, using the Schaefer parcellation atlas. DAN, dorsal attention network; DMN, default mode network; FPN, fronto-parietal network; FTP, flortaucipir tracer; LIM, limbic network; NAV, Navidea tracer; SAL, salience network; SM, somatomotor network; VAN, ventral attention network and VIS, visual network. * $p<0.05$, ** $p<0.01$. Results that survived correction for false discovery rate are indicated by FDR.

3.5. Association between AD-pathological biomarkers and RSFC

In the PET subsample, we found no association between global A*β* deposition or *tau* deposition in the entorhinal cortex with baseline RSFC (all *p*'s > 0.05, data not shown) nor with RSFC changes over time, using any of the three parcellations (**Supplemental Table S6, *S7* and S8**). Looking at the strength of the associations (*t*-values), no association would have reached significance even with a sample size of 247 participants (full cohort).

4. Discussion

We investigated the impact of baseline cholesterol and blood pressure, as well as AD-related biomarkers on longitudinal RSFC changes within a well-established set of predefined functional networks covering the entire cortex. The current study provides evidence that vascular burden contributes to RSFC trajectories in middle-to-late life adulthood. While RSFC was quite stable or slightly increased across a 4-year follow-up (interquartile range 2-4 years), higher total- and LDL-cholesterol lev-

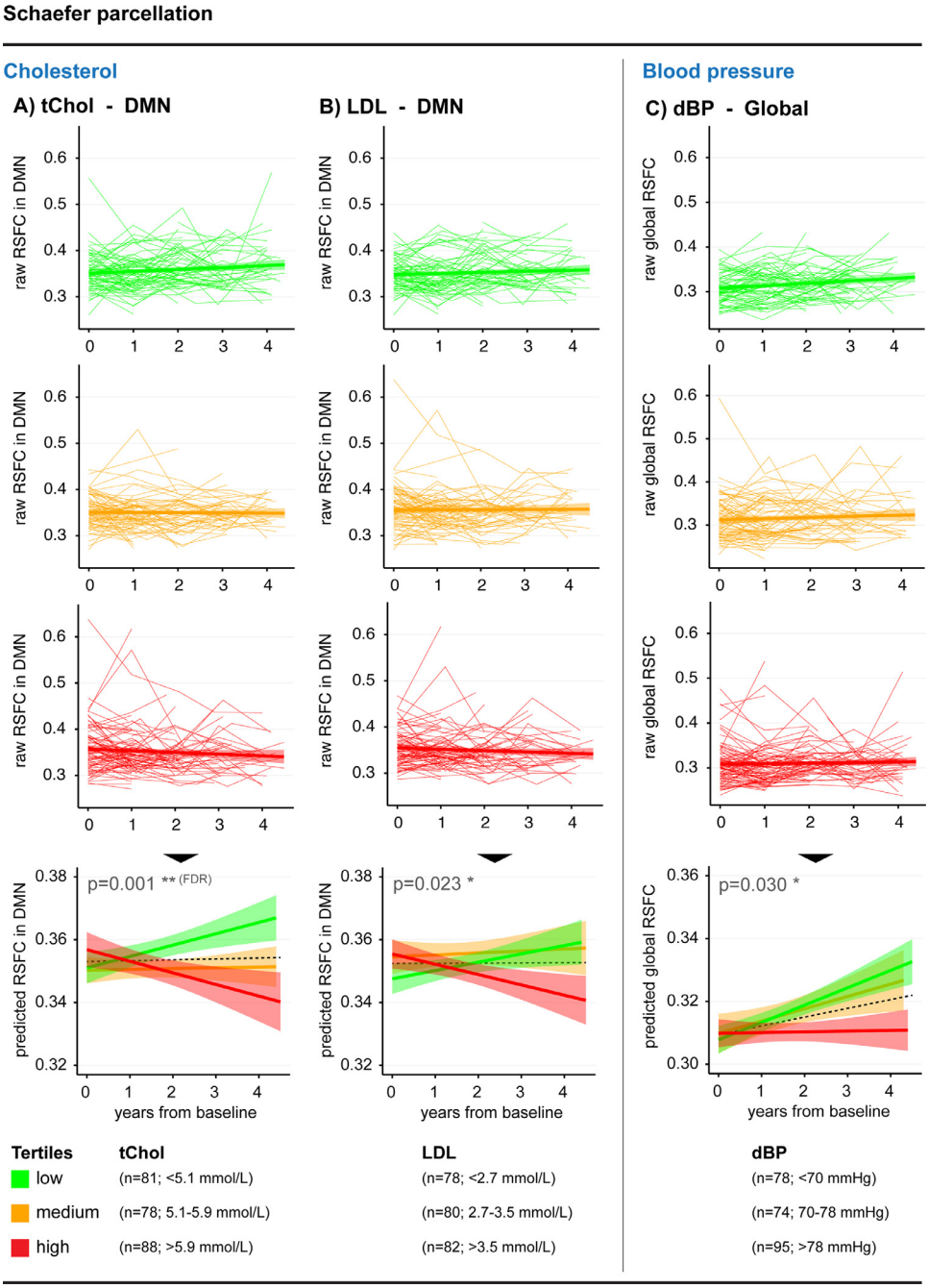

Fig. 3. *Change in resting-state functional connectivity, assessed using the Schaefer brain parcellation, as a function of vascular risk factors.* These graphs are a longitudinal representation of a subset of the results shown in Fig. 2. Results were only plotted when significant results were replicated with at least one other parcellation (MIST or Power). Continuous measures of (A) tChol, (B) LDL-cholesterol and (C) dBP were divided into tertiles for better visualization only. The small lines in the upper three rows of panels represent individual raw RSFC trajectories plotted against follow-up time from baseline for low (green), medium (orange) and high (red) vascular risk factor tertiles, respectively. In the lowest row of panels, predicted RSFC estimates, derived from linear-mixed effects models, are shown. Shaded regions represent 95% confidence intervals. Results that survived correction for false discovery rate are indicated by FDR. The dotted black lines in the lowest row of panels represent the mean change in RSFC across all individuals. dBP, diastolic blood pressure; DMN, default mode network; LDL, low-density lipoprotein; RSFC, resting-state functional connectivity; tChol, total-cholesterol.

els were associated with reductions in DMN RSFC over time, whereas higher diastolic blood pressure was associated with reduced whole-brain RSFC. In contrast, *APOE ε4* and AD-related biomarkers showed no association with RSFC changes over time. These last analyses were only performed in a subset of the cohort and will therefore need to be replicated. VRFs may partially explain the decrease in RSFC usually associated with older age. Both cholesterol and blood pressure were tested in the same statistical models, so these two vascular factors likely contribute to RSFC changes via somewhat independent mechanisms (Charmichael et al., 2014).

We found an association of higher total- and LDL-cholesterol levels with a reduction in RSFC, specifically within the DMN, whereas other functional networks showed no consistent changes in RSFC linked to cholesterol levels. It has been suggested that the DMN has the highest metabolic rate in the brain and is involved in a large variety of demanding cognitive tasks (Raichle et al., 2001; Vaishnavi et al., 2010; Yang et al., 2016; Rashid et al., 2019). This high economical load may render the DMN preferentially vulnerable to aging and AD in comparison to other functional networks (Hedden et al., 2009; Sheline et al., 2010). Elevated vascular risk, measured via composite VRF measures, has been associated with a reduction in glucose metabolism (Kuczynski et al., 2009), resting cerebral blood flow (Beason-Held et al., 2012) and cerebrovascular reactivity in DMN regions (Tchistiakova et al., 2015). These vascular effects might evolve gradually in the presence of chronically elevated cholesterol levels and lead to disturbed brain functions. In comparison to other networks, RSFC seems to be related to cerebrovascular integrity particularly within the DMN (Sun et al., 2011; Hoogenboom et al., 2014). In line with this, a decrease in RSFC (Sun et al., 2011) and functional connectivity density (Yi et al., 2012) in the DMN has been found in patients with mild cogni-

tive impairment and moderate to severe white matter hyperintensities, a measure of vascular brain integrity.

A reduction of DMN RSFC with advancing age has been recently shown in a longitudinal study of healthy older adults aged 60 years and older (Ng et al., 2016), a finding that was not replicated in our cohort. In contrast, our data suggests no change of DMN RSFC over time in the general cohort. When dividing the individuals by VRF profile, we found an increased change or no change in DMN RSFC in individuals with lower to moderate cholesterol levels, whereas we found a decline in DMN RSFC in the presence of high total- and LDL-cholesterol burden (see low, medium and high tertiles slopes in **Fig. 3**). These differential trajectories highlight the relevant contribution of high VRFs to detect a decline in RSFC in cognitively unimpaired older adults. Decline in DMN RSFC has also been repetitively associated with clinical AD (Badhwar et al., 2017). While we found no association between AD pathology and changes in RSFC, VRFs might nevertheless increase vulnerability to AD by creating early brain alteration in individuals at risk of AD. It has also been described that VRFs may influence AD risk via AD-independent pathways (Zlokovic, 2011; Villeneuve et al., 2015). Additionally, the association between AD pathology and RSFC changes might only be detectable later in the disease course. Our participants were all cognitively normal and relatively young (mean age of 63 years) compared to other cohorts that have found such associations (Elman et al., 2016).

Researchers have recently begun to investigate not only network-based RSFC, but also global RSFC (i.e. connectivity of each grey matter region with all other grey matter regions), as both seem to represent complementary predictors of AD pathologies and their propagation (Mutlu et al., 2017; Staffaroni et al., 2018). Brain regions with high global RSFC are proposed to represent hub regions in the brain, many of which are located within the DMN, showing especially high metabolic activity, neuronal activity and vulnerability to AD pathologies (Buckner et al., 2009; Staffaroni et al., 2018). While higher cholesterol levels showed network-specific associations with reduction in RSFC, higher diastolic, but not systolic, blood pressure was associated with reduction of global RSFC over time. Diastolic hypertension may specifically accelerate age-related sclerotic changes in small arterioles spread across the brain (Englund et al., 1988), leading to reduced cerebral perfusion, white matter lesions, atrophy and finally cognitive impairment (de Leeuw et al., 1999; den Heijer et al., 2005; Tsivgoulis et al., 2009). Among different peripheral VRF, high blood pressure is strongly associated with vascular brain pathologies, i.e., white matter hyperintensities, possibly damaging cerebral microcirculation (Moroni et al., 2018). While in contrast the role of dyslipidemia in vascular brain pathologies remains not well understood, treatment of both hypertension and dyslipidemia seems to be a promising avenue to slow down the progression in vascular brain pathologies (Richard et al., 2010) and thus potentially in pathological functional alterations (Jaywant et al., 2020). It has further been suggested that diastolic blood pressure is associated with structural impairment earlier on than systolic blood pressure; a similar time course may appear for functional impairment (Power et al., 2016).

Finally, we found increases in network and global RSFC over time across all individuals without taking VRF differences into account. This hyperconnectivity has been reported in previous studies (Hillary et al., 2017; Staffaroni et al., 2018; Verfaillie et al., 2018) and has been typically interpreted as a compensatory mechanism to maintain cognitive function that starts to be compromised with aging and early AD (Mormino et al., 2011). Newer concepts posit that neurons in the DMN might be unable to handle costly metabolic alterations due to higher pathology-induced processing burden, leading to a transfer of processing burden to downstream regions and/or noisy inefficient synaptic communications, which results in a short-term hyperconnectivity (Jones et al., 2016; Hillary et al., 2017). Particularly, most central and metabolically active hub regions are likely to express increased connectivity (Hillary et al., 2017). Increases in RSFC have been proposed to occur until individuals reach an age of ~74 years, after which a decline in RSFC begins (Staffaroni et al., 2018). Our study with relatively young older adults suggests that such a cascading network failure might be accelerated in the presence of VRFs, by preluding the tipping point where high VRF burden overwhelms neurons of hub regions, resulting in functional disconnection.

The links between inter- and intra-network connectivity and health-related outcomes are still not fully established. Some recent studies have reported positive relationships between intra-network RSFC and cognitive function across the adult life span (Varangis et al., 2019), in cognitively unimpaired older adults (Staffaroni et al., 2018), as well as in the context of Alzheimer's disease (Badhwar et al., 2017). Interestingly, these associations between cognitive function and RSFC are most consistently found within the DMN. Nevertheless, more work is needed to address if and how changes in RSFC, as shown here in the context of high VRFs, serve as a valid clinical marker in healthy aging and neurodegenerative diseases.

In our cohort of cognitively normal individuals with increased risk for AD, we found associations between higher VRFs and a decrease in RSFC over time. We did not find associations of AD pathology with changes in RSFC in the PET subsample. One could hypothesize from previous studies (Hedden et al., 2009; Franzmeier et al., 2019; Schultz et al., 2020) that an AD pathology–RSFC association develops later in the AD process.

A strength of our study is its longitudinal design to assess trajectories of functional connectivity in the context of vascular- and incipient AD-related burden in cognitively normal individuals. Since RSFC was measured prospectively from the time point of VRF assessment, it can be hypothesised that VRFs may induce changes in RSFC, although this needs to be proven by future interventional trials. The reproduction of our results using 3 different parcellation atlases further strengthens their validity. There are also several caveats that must be taken into consideration when interpreting our findings. First, blood pressure values were assessed only from one measurement instead of averaging values of multiple measurements at baseline. Second, family history of AD was ascertained via participant self-report, leaving a degree of uncertainty to the diagnosis of AD-specific dementia. Third, we used peripheral measures to assess cholesterol and blood pressure levels. 24S-hydroxycholesterol (the predominant metabolite of brain cholesterol), cerebral perfusion pressure or measures of cerebrovascular impairment (i.e. white matter lesions, lacunes, and microbleeds) may provide more direct evidence about a relationship between vascular burden, vascular brain injuries and changes in RSFC. Fourth, our sample was only very mildly affected by other common VRFs, such as diabetes, smoking and obesity, and therefore these factors still need to be assessed in future studies. Nevertheless, the presence of VRFs in our participants was in general comparable to the US population (Ford et al., 2004), except that current smoking was on average 10-fold lower in the PREVENT-AD cohort, suggesting that our results are extendible to further populations. Fifth, levels of cerebral AD-related PET biomarkers were low to moderate in our relatively young cohort and the sample size was limited, therefore, associations of Aβ and *tau* with longitudinal RSFC may have been harder to detect.

5. Conclusion

In sum, our results suggest a significant contribution of cholesterol to changes in DMN and blood pressure to changes in global RSFC in cognitively normal older adults. In our cohort that includes only relatively young cognitively normal older adults with an elevated risk to develop AD, we found no effect of Aβ or *tau* on RSFC changes, suggesting that the link between these pathologies on changes in RSFC might only be captured later in the course of the disease. It will be of interest to follow these individuals over time to assess when increasing AD pathology starts to impair RSFC and if VRFs and Aβ/*tau* burden have an additive or a synergistic effect on brain functional connectivity.

Declaration of Competing Interest

The authors declare no competing financial conflicts of interests.

Funding

This work was supported by the Alzheimer Society of Canada, Brain Canada, Quebec Bio-Imaging Network, Healthy Brains for Healthy Lives, the Alzheimer's Association, McGill University, the Fonds de Recherche du Québec – Santé (FRQ-S), an unrestricted research grant from Pfizer Canada, the Levesque Foundation, the Douglas Hospital Research Centre and Foundation, the Canada Institutes of Health Research, the Canada Fund for Innovation, and the German Research Foundation (DFG).

Acknowledgments

The authors wish to acknowledge the PREVENT-AD staff, especially Jennifer Tremblay-Mercier, Joanne Frenette, Leslie-Ann Daoust, and the Brain Imaging Center of the Douglas Mental Health Research Institute, and the PET and cyclotron units of the Montreal Neurological Institute. A full listing of the PREVENT-AD Research Group members can be found at https://preventad.loris.ca/acknowledgements/acknowledgements.php?date=[2018-11-14]. We would also like to acknowledge the participants of the PREVENT-AD cohort for dedicating their time and energy to helping us collect these data.

Author Contributions

Theresa Köbe: study concept and design, analysis and interpretation of data, drafting and revising the manuscript for intellectual content; **Alexa Pichet Binette**: data acquisition and analysis, revising the manuscript for intellectual content; **Jacob W. Vogel**: data analysis, revising the manuscript for intellectual content; **Pierre-François Meyer**: data analysis, revising the manuscript for intellectual content; **John Breitner**: acquisition of data, protocol concept and design, revising the manuscript for intellectual content; **Judes Poirier**: acquisition of data, protocol concept and design, revising the manuscript for intellectual content; **Sylvia Villeneuve**: acquisition of data, study concept and design, interpretation of data, revision of manuscript for intellectual content.

Supplementary materials

Supplementary material associated with this article can be found, in the online version, at doi:10.1016/j.neuroimage.2021.117832.

References

Badhwar, A., Tam, A., Dansereau, C., Orban, P., Hoffstaedter, F., Bellec, P., 2017. Resting-state network dysfunction in Alzheimer's disease: a systematic review and meta-analysis. Alzheimers Dement. 8, 73–85. doi:10.1016/j.dadm.2017.03.007.

Baker, S.L., Maass, A., Jagust, W.J., 2017. Considerations and code for partial volume correcting [(18)F]-AV-1451 tau PET data. Data Brief 15, 648–657. doi:10.1016/j.dib.2017.10.024.

Bates, D., Maechler, M., Bolker, B., Walker, S., 2015. Fitting linear mixed-effects models using lme4. J. Stat. Softw. 67, 1–48.

Beason-Held, L.L., Thambisetty, M., Deib, G., Sojkova, J., Landman, B.A., Zonderman, A.B., Ferrucci, L., Kraut, M.A., Resnick, S.M., 2012. Baseline cardiovascular risk predicts subsequent changes in resting brain function. Stroke 43, 1542–1547. doi:10.1161/STROKEAHA.111.638437.

Betzel, R.F., Byrge, L., He, Y., Goni, J., Zuo, X.N., Sporns, O., 2014. Changes in structural and functional connectivity among resting-state networks across the human lifespan. Neuroimage 102 (Pt 2), 345–357. doi:10.1016/j.neuroimage.2014.07.067.

Breitner, J.C.S., Poirier, J., Etienne, P.E., Leoutsakos, J.M., 2016. Rationale and structure for a new center for studies on prevention of Alzheimer's disease (StoP-AD). J. Prev. Alzheimers Dis. 3, 236–242. doi:10.14283/jpad.2016.121.

Brier, M.R., Thomas, J.B., Snyder, A.Z., Benzinger, T.L., Zhang, D., Raichle, M.E., Holtzman, D.M., Morris, J.C., Ances, B.M., 2012. Loss of intranetwork and internetwork resting state functional connections with Alzheimer's disease progression. J. Neurosci. 32, 8890–8899. doi:10.1523/JNEUROSCI.5698-11.2012.

Buckner, R.L., Sepulcre, J., Talukdar, T., Krienen, F.M., Liu, H., Hedden, T., Andrews-Hanna, J.R., Sperling, R.A., Johnson, K.A., 2009. Cortical hubs revealed by intrinsic functional connectivity: mapping, assessment of stability, and relation to Alzheimer's disease. J. Neurosci. 29, 1860–1873. doi:10.1523/JNEUROSCI.5062-08.2009.

Carmichael, O., 2014. Preventing vascular effects on brain injury and cognition late in life: knowns and unknowns. Neuropsychol. Rev. 24, 371–387. doi:10.1007/s11065-014-9264-7.

de Leeuw, F.E., de Groot, J.C., Oudkerk, M., Witteman, J.C., Hofman, A., van Gijn, J., Breteler, M.M., 1999. A follow-up study of blood pressure and cerebral white matter lesions. Ann. Neurol. 46, 827–833. doi:10.1002/1531-8249(199912)46:6<827, aid-ana4>3.3.co;2-8.

den Heijer, T., Launer, L.J., Prins, N.D., van Dijk, E.J., Vermeer, S.E., Hofman, A., Koudstaal, P.J., Breteler, M.M., 2005. Association between blood pressure, white matter lesions, and atrophy of the medial temporal lobe. Neurology 64, 263–267. doi:10.1212/01.WNL.0000149641.55751.2E.

Desikan, R.S., Segonne, F., Fischl, B., Quinn, B.T., Dickerson, B.C., Blacker, D., Buckner, R.L., Dale, A.M., Maguire, R.P., Hyman, B.T., Albert, M.S., Killiany, R.J., 2006. An automated labeling system for subdividing the human cerebral cortex on MRI scans into gyral based regions of interest. Neuroimage 31, 968–980. doi:10.1016/j.neuroimage.2006.01.021.

Elman, J.A., Madison, C.M., Baker, S.L., Vogel, J.W., Marks, S.M., Crowley, S., O'Neil, J.P., Jagust, W.J., 2016. Effects of beta-amyloid on resting state functional connectivity within and between networks reflect known patterns of regional vulnerability. Cereb. Cortex 26, 695–707. doi:10.1093/cercor/bhu259.

Englund, E., Brun, A., Alling, C., 1988. White matter changes in dementia of Alzheimer's type. Biochemical and neuropathological correlates. Brain 111 (Pt 6), 1425–1439. doi:10.1093/brain/111.6.1425.

Fatima, S., Ijaz, A., Sharif, T.B., Khan, D.A., Siddique, A., 2016. Accuracy of non-fasting lipid profile for the assessment of lipoprotein coronary risk. J. Coll. Phys. Surg. Pak 26, 954–957 2493.

Ford, E.S., Giles, W.H., Mokdad, A.H., 2004. The distribution of 10-Year risk for coronary heart disease among US adults: findings from the National Health and Nutrition Examination Survey III. J. Am. Coll. Cardiol. 43, 1791–1796. doi:10.1016/j.jacc.2003.11.061.

Franzmeier, N., Rubinski, A., Neitzel, J., Kim, Y., Damm, A., Na, D.L., Kim, H.J., Lyoo, C.H., Cho, H., Finsterwalder, S., Duering, M., Seo, S.W., Ewers, M., 2019. Functional connectivity associated with tau levels in ageing, Alzheimer's, and small vessel disease. Brain 142, 1093–1107. doi:10.1093/brain/awz026.

Goldman, J.S., Hahn, S.E., Catania, J.W., LaRusse-Eckert, S., Butson, M.B., Rumbaugh, M., Strecker, M.N., Roberts, J.S., Burke, W., Mayeux, R., Bird, T., 2011. Genetic counseling and testing for Alzheimer disease: joint practice guidelines of the American College of Medical Genetics and the National Society of Genetic Counselors. Genet. Med. 13, 597–605. doi:10.1097/GIM.0b013e31821d69b8.

Haight, T.J., Bryan, R.N., Erus, G., Davatzikos, C., Jacobs, D.R., D'Esposito, M., Lewis, C.E., Launer, L.J., 2015. Vascular risk factors, cerebrovascular reactivity, and the default-mode brain network. Neuroimage 115, 7–16. doi:10.1016/j.neuroimage.2015.04.039.

Hedden, T., Van Dijk, K.R., Becker, J.A., Mehta, A., Sperling, R.A., Johnson, K.A., Buckner, R.L., 2009. Disruption of functional connectivity in clinically normal older adults harboring amyloid burden. J. Neurosci. 29, 12686–12694. doi:10.1523/JNEUROSCI.3189-09.2009, 29/40/12686 [pii].

Hillary, F.G., Grafman, J.H., 2017. Injured Brains and Adaptive Networks: The Benefits and Costs of Hyperconnectivity. Trends Cogn. Sci. 21, 385–401. doi:10.1016/j.tics.2017.03.003.

Hohenfeld, C., Werner, C.J., Reetz, K., 2018. Resting-state connectivity in neurodegenerative disorders: Is there potential for an imaging biomarker? Neuroimage Clin 18, 849–870. doi:10.1016/j.nicl.2018.03.013.

Hoogenboom, W.S., Marder, T.J., Flores, V.L., Huisman, S., Eaton, H.P., Schneiderman, J.S., Bolo, N.R., Simonson, D.C., Jacobson, A.M., Kubicki, M., Shenton, M.E., Musen, G., 2014. Cerebral white matter integrity and resting-state functional connectivity in middle-aged patients with type 2 diabetes. Diabetes 63, 728–738. doi:10.2337/db13-1219.

Iturria-Medina, Y., Sotero, R.C., Toussaint, P.J., Mateos-Perez, J.M., Evans, A.C., 2016. Early role of vascular dysregulation on late-onset Alzheimer's disease based on multifactorial data-driven analysis. Nat. Commun. 7, 11934. doi:10.1038/ncomms11934.

Jaywant, A., K. Dunlop, L. W. Victoria, L. Oberlin, C. Lynch, M. Respino, A. Kuceyeski, M. Scult, M. Hoptman, C. Liston, M. W. O'Dell, G. S. Alexopoulos and F. M. Gunning (2020) White matter hyperintensity-associated structural disconnection, resting state functional connectivity, and cognitive control in older adults. *bioRxiv*. 10.1101/2020.04.14.039065

Jones, D.T., Knopman, D.S., Gunter, J.L., Graff-Radford, J., Vemuri, P., Boeve, B.F., Petersen, R.C., Weiner, M.W., Jack Jr., C.R., 2016. Cascading network failure across the Alzheimer's disease spectrum. Brain 139, 547–562. doi:10.1093/brain/awv338.

Kannel, W.B., Vasan, R.S., 2009. Is age really a non-modifiable cardiovascular risk factor? Am. J. Cardiol. 104, 1307–1310. doi:10.1016/j.amjcard.2009.06.051.

Köbe, T., Gonneaud, J., Pichet Binette, A., Meyer, P.F., McSweeney, M., Rosa-Neto, P., Breitner, J.C.S., Poirier, J., Villeneuve, S., Presymptomatic Evaluation of Experimental or Novel Treatments for Alzheimer Disease Research, G., 2020. Association of vascular risk factors with beta-amyloid peptide and tau burdens in cognitively unimpaired individuals and its interaction with vascular medication use. JAMA Netw. Open 3, e1920780. doi:10.1001/jamanetworkopen.2019.20780.

Kuczynski, B., Jagust, W., Chui, H.C., Reed, B., 2009. An inverse association of cardiovascular risk and frontal lobe glucose metabolism. Neurology 72, 738–743. doi:10.1212/01.wnl.0000343005.35498.e5.

Langsted, A., Nordestgaard, B.G., 2019. Nonfasting versus fasting lipid profile for cardiovascular risk prediction. Pathology 51, 131–141. doi:10.1016/j.pathol.2018.09.062.

Li, X., Liang, Y., Chen, Y., Zhang, J., Wei, D., Chen, K., Shu, N., Reiman, E.M., Zhang, Z., 2015. Disrupted frontoparietal network mediates white matter structure dysfunction associated with cognitive decline in hypertension patients. J. Neurosci. 35, 10015–10024. doi:10.1523/JNEUROSCI.5113-14.2015.

Liu, T.T., 2013. Neurovascular factors in resting-state functional MRI. Neuroimage 80, 339–348. doi:10.1016/j.neuroimage.2013.04.071.

Marwick, B., Krishnamoorthy, K., 2019. cvequality: Tests for the Equality of Coefficients of Variation from Multiple Groups. https://github.com/benmarwick/cvequality.

McKay, G.J., Silvestri, G., Chakravarthy, U., Dasari, S., Fritsche, L.G., Weber, B.H., Keilhauer, C.N., Klein, M.L., Francis, P.J., Klaver, C.C., Vingerling, J.R., Ho, L., De Jong, P.T., Dean, M., Sawitzke, J., Baird, P.N., Guymer, R.H., Stambolian, D., Orlin, A., Seddon, J.M., Peter, I., Wright, A.F., Hayward, C., Lotery, A.J., Ennis, S., Gorin, M.B., Weeks, D.E., Kuo, C.L., Hingorani, A.D., Sofat, R., Cipriani, V., Swaroop, A., Othman, M., Kanda, A., Chen, W., Abecasis, G.R., Yates, J.R., Webster, A.R., Moore, A.T., Seland, J.H., Rahu, M., Soubrane, G., Tomazzoli, L., Topouzis, F., Vioque, J., Young, I.S., Fletcher, A.E., Patterson, C.C., 2011. Variations in apolipoprotein E frequency with age in a pooled analysis of a large group of older people. Am. J. Epidemiol. 173, 1357–1364. doi:10.1093/aje/kwr015.

McSweeney, M., Pichet Binette, A., Meyer, P.F., Gonneaud, J., Bedetti, C., Ozlen, H., Labonte, A., Rosa-Neto, P., Breitner, J., Poirier, J., Villeneuve, S.P.-A. R. Group, 2020. Intermediate flortaucipir uptake is associated with Abeta-PET and CSF tau in asymptomatic adults. Neurology 94, e1190–e1200. doi:10.1212/WNL.0000000000008905.

Meyer, P.F., Savard, M., Poirier, J., Labonte, A., Rosa-Neto, P., Weitz, T.M., Town, T., Breitner, J., 2018. Bi-directional Association of Cerebrospinal Fluid Immune Markers with Stage of Alzheimer's Disease Pathogenesis. J. Alzheimers Dis. 63, 577–590. doi:10.3233/JAD-170887.

Mormino, E.C., Smiljic, A., Hayenga, A.O., Onami, S.H., Greicius, M.D., Rabinovici, G.D., Janabi, M., Baker, S.L., Yen, I.V., Madison, C.M., Miller, B.L., Jagust, W.J., 2011. Relationships between beta-amyloid and functional connectivity in different components of the default mode network in aging. Cereb. Cortex 21, 2399–2407. doi:10.1093/cercor/bhr025.

Moroni, F., Ammirati, E., Rocca, M.A., Filippi, M., Magnoni, M., Camici, P.G., 2018. Cardiovascular disease and brain health: Focus on white matter hyperintensities. Int J Cardiol Heart Vasc 19, 63–69. doi:10.1016/j.ijcha.2018.04.006.

Morris, J.C., 1993. The Clinical Dementia Rating (CDR): current version and scoring rules. Neurology 43, 2412–2414.

Murphy, K., Birn, R.M., Handwerker, D.A., Jones, T.B., Bandettini, P.A., 2009. The impact of global signal regression on resting state correlations: are anti-correlated networks introduced? Neuroimage 44, 893–905. doi:10.1016/j.neuroimage.2008.09.036.

Mutlu, J., Landeau, B., Gaubert, M., de La Sayette, V., Desgranges, B., Chetelat, G., 2017. Distinct influence of specific versus global connectivity on the different Alzheimer's disease biomarkers. Brain 140, 3317–3328. doi:10.1093/brain/awx279.

Myers, N., Pasquini, L., Gottler, J., Grimmer, T., Koch, K., Ortner, M., Neitzel, J., Muhlau, M., Forster, S., Kurz, A., Forstl, H., Zimmer, C., Wohlschlager, A.M., Riedl, V., Drzezga, A., Sorg, C., 2014. Within-patient correspondence of amyloid-beta and intrinsic network connectivity in Alzheimer's disease. Brain 137, 2052–2064. doi:10.1093/brain/awu103.

Nasreddine, Z.S., Phillips, N.A., Bedirian, V., Charbonneau, S., Whitehead, V., Collin, I., Cummings, J.L., Chertkow, H., 2005. The Montreal Cognitive Assessment, MoCA: a brief screening tool for mild cognitive impairment. J. Am. Geriatr. Soc. 53, 695–699. doi:10.1111/j.1532-5415.2005.53221.x.

Ng, K.K., Lo, J.C., Lim, J.K.W., Chee, M.W.L., Zhou, J., 2016. Reduced functional segregation between the default mode network and the executive control network in healthy older adults: A longitudinal study. Neuroimage 133, 321–330. doi:10.1016/j.neuroimage.2016.03.029.

Orban, P., Madjar, C., Savard, M., Dansereau, C., Tam, A., Das, S., Evans, A.C., Rosa-Neto, P., Breitner, J.C., Bellec, P., Group, P.-A.R., 2015. Test-retest resting-state fMRI in healthy elderly persons with a family history of Alzheimer's disease. Sci. Data 2, 150043. doi:10.1038/sdata.2015.43.

Palmqvist, S., Scholl, M., Strandberg, O., Mattsson, N., Stomrud, E., Zetterberg, H., Blennow, K., Landau, S., Jagust, W., Hansson, O., 2017. Earliest accumulation of beta-amyloid occurs within the default-mode network and concurrently affects brain connectivity. Nat. Commun. 8, 1214. doi:10.1038/s41467-017-01150-x.

Power, J.D., Barnes, K.A., Snyder, A.Z., Schlaggar, B.L., Petersen, S.E., 2012. Spurious but systematic correlations in functional connectivity MRI networks arise from subject motion. Neuroimage 59, 2142–2154. doi:10.1016/j.neuroimage.2011.10.018.

Power, J.D., Cohen, A.L., Nelson, S.M., Wig, G.S., Barnes, K.A., Church, J.A., Vogel, A.C., Laumann, T.O., Miezin, F.M., Schlaggar, B.L., Petersen, S.E., 2011. Functional network organization of the human brain. Neuron 72, 665–678. doi:10.1016/j.neuron.2011.09.006.

Power, M.C., Schneider, A.L., Wruck, L., Griswold, M., Coker, L.H., Alonso, A., Jack Jr., C.R., Knopman, D., Mosley, T.H., Gottesman, R.F., 2016. Life-course blood pressure in relation to brain volumes. Alzheimers Dement. 12, 890–899. doi:10.1016/j.jalz.2016.03.012.

Raichle, M.E., MacLeod, A.M., Snyder, A.Z., Powers, W.J., Gusnard, D.A., Shulman, G.L., 2001. A default mode of brain function. Proc. Natl. Acad. Sci. U. S. A. 98, 676–682. doi:10.1073/pnas.98.2.676.

Randolph, C., Tierney, M.C., Mohr, E., Chase, T.N., 1998. The Repeatable Battery for the Assessment of Neuropsychological Status (RBANS): preliminary clinical validity. J. Clin. Exp. Neuropsychol. 20, 310–319. doi:10.1076/jcen.20.3.310.823.

Rashid, B., Dev, S.I., Esterman, M., Schwarz, N.F., Ferland, T., Fortenbaugh, F.C., Milberg, W.P., McGlinchey, R.E., Salat, D.H., Leritz, E.C., 2019. Aberrant patterns of default-mode network functional connectivity associated with metabolic syndrome: a resting-state study. Brain Behav e01333. doi:10.1002/brb3.1333.

Richard, E., Gouw, A.A., Scheltens, P., van Gool, W.A., 2010. Vascular care in patients with Alzheimer disease with cerebrovascular lesions slows progression of white matter lesions on MRI: the evaluation of vascular care in Alzheimer's disease (EVA) study. Stroke 41, 554–556. doi:10.1161/STROKEAHA.109.571281.

Rifai, N., Young, I.S., Nordestgaard, B.G., Wierzbicki, A.S., Vesper, H., Mora, S., Stone, N.J., Genest, J., Miller, G., 2016. Nonfasting sample for the determination of routine lipid profile: is it an idea whose time has come? Clin. Chem. 62, 428–435. doi:10.1373/clinchem.2015.247866.

Rodrigue, K.M., Rieck, J.R., Kennedy, K.M., Devous Sr., M.D., Diaz-Arrastia, R., Park, D.C., 2013. Risk factors for beta-amyloid deposition in healthy aging: vascular and genetic effects. JAMA Neurol. 70, 600–606. doi:10.1001/jamaneurol.2013.1342.

Schaefer, A., Kong, R., Gordon, E.M., Laumann, T.O., Zuo, X.N., Holmes, A.J., Eickhoff, S.B., Yeo, B.T.T., 2018. Local-global parcellation of the human cerebral cortex from intrinsic functional connectivity MRI. Cereb. Cortex 28, 3095–3114. doi:10.1093/cercor/bhx179.

Schöll, M., Lockhart, S.N., Schonhaut, D.R., O'Neil, J.P., Janabi, M., Ossenkoppele, R., Baker, S.L., Vogel, J.W., Faria, J., Schwimmer, H.D., Rabinovici, G.D., Jagust, W.J., 2016. PET imaging of tau deposition in the aging human brain. Neuron 89, 971–982. doi:10.1016/j.neuron.2016.01.028.

Schultz, A.P., Buckley, R.F., Hampton, O.L., Scott, M.R., Properzi, M.J., Pena-Gomez, C., Pruzin, J.J., Yang, H.S., Johnson, K.A., Sperling, R.A., Chhatwal, J.P., 2020. Longitudinal degradation of the default/salience network axis in symptomatic individuals with elevated amyloid burden. Neuroimage Clin 26, 102052. doi:10.1016/j.nicl.2019.102052.

Sheline, Y.I., Raichle, M.E., Snyder, A.Z., Morris, J.C., Head, D., Wang, S., Mintun, M.A., 2010. Amyloid plaques disrupt resting state default mode network connectivity in cognitively normal elderly. Biol. Psychiatry 67, 584–587. doi:10.1016/j.biopsych.2009.08.024.

Small, S.A., Duff, K., 2008. Linking Abeta and tau in late-onset Alzheimer's disease: a dual pathway hypothesis. Neuron 60, 534–542. doi:10.1016/j.neuron.2008.11.007.

Staffaroni, A.M., Brown, J.A., Casaletto, K.B., Elahi, F.M., Deng, J., Neuhaus, J., Cobigo, Y., Mumford, P.S., Walters, S., Saloner, R., Karydas, A., Coppola, G., Rosen, H.J., Miller, B.L., Seeley, W.W., Kramer, J.H., 2018. The longitudinal trajectory of default mode network connectivity in healthy older adults varies as a function of age and is associated with changes in episodic memory and processing speed. J. Neurosci. 38, 2809–2817. doi:10.1523/JNEUROSCI.3067-17.2018.

Sun, Y.W., Qin, L.D., Zhou, Y., Xu, Q., Qian, L.J., Tao, J., Xu, J.R., 2011. Abnormal functional connectivity in patients with vascular cognitive impairment, no dementia: a resting-state functional magnetic resonance imaging study. Behav. Brain Res. 223, 388–394. doi:10.1016/j.bbr.2011.05.006.

Tam, A., Dansereau, C., Badhwar, A., Orban, P., Belleville, S., Chertkow, H., Dagher, A., Hanganu, A., Monchi, O., Rosa-Neto, P., Shmuel, A., Wang, S., Breitner, J., Bellec, P., 2015. Common effects of amnestic mild cognitive impairment on resting-state connectivity across four independent studies. Front. Aging Neurosci. 7, 242. doi:10.3389/fnagi.2015.00242.

Tchistiakova, E., Crane, D.E., Mikulis, D.J., Anderson, N.D., Greenwood, C.E., Black, S.E., MacIntosh, B.J., 2015. Vascular risk factor burden correlates with cerebrovascular reactivity but not resting state coactivation in the default mode network. J. Magn. Reson. Imaging 42, 1369–1376. doi:10.1002/jmri.24917.

Tsivgoulis, G., Alexandrov, A.V., Wadley, V.G., Unverzagt, F.W., Go, R.C., Moy, C.S., Kissela, B., Howard, G., 2009. Association of higher diastolic blood pressure levels with cognitive impairment. Neurology 73, 589–595. doi:10.1212/WNL.0b013e3181b38969.

Urchs, S., Armoza, J., Moreau, C., Benhajali, Y., St-Aubin, J., Orban, P., Bellec, P., 2019. MIST: A multi-resolution parcellation of functional brain networks [version 2; peer review: 4 approved]. MNI Open Res 1, 3.

Vachon-Presseau, E., Berger, S.E., Abdullah, T.B., Griffith, J.W., Schnitzer, T.J., Apkarian, A.V., 2019. Identification of traits and functional connectivity-based neurotraits of chronic pain. PLoS Biol. 17, e3000349. doi:10.1371/journal.pbio.3000349.

Vaishnavi, S.N., Vlassenko, A.G., Rundle, M.M., Snyder, A.Z., Mintun, M.A., Raichle, M.E., 2010. Regional aerobic glycolysis in the human brain. Proc. Natl. Acad. Sci. U. S. A. 107, 17757–17762. doi:10.1073/pnas.1010459107.

Varangis, E., Habeck, C.G., Razlighi, Q.R., Stern, Y., 2019. The effect of aging on resting state connectivity of predefined networks in the brain. Front. Aging Neurosci. 11, 234. doi:10.3389/fnagi.2019.00234.

Verfaillie, S.C.J., Pichet Binette, A., Vachon-Presseau, E., Tabrizi, S., Savard, M., Bellec, P., Ossenkoppele, R., Scheltens, P., van der Flier, W.M., Breitner, J.C.S., Villeneuve, S., Group, P.-A.R., 2018. Subjective cognitive decline is associated with altered default mode network connectivity in individuals with a family history of Alzheimer's disease. Biol. Psychiatry Cogn. Neurosci. Neuroimaging 3, 463–472. doi:10.1016/j.bpsc.2017.11.012.

Villeneuve, S., Jagust, W.J., 2015. Imaging vascular disease and amyloid in the aging brain: implications for treatment. J. Prev. Alzheimers Dis. 2, 64–70. doi:10.14283/jpad.2015.47.

Villeneuve, S., Rabinovici, G.D., Cohn-Sheehy, B.I., Madison, C., Ayakta, N., Ghosh, P.M., La Joie, R., Arthur-Bentil, S.K., Vogel, J.W., Marks, S.M., Lehmann, M., Rosen, H.J., Reed, B., Olichney, J., Boxer, A.L., Miller, B.L., Borys, E., Jin, L.W., Huang, E.J., Grinberg, L.T., DeCarli, C., Seeley, W.W., Jagust, W., 2015. Existing Pittsburgh Compound-B positron emission tomography thresholds are too high: statistical and pathological evaluation. Brain 138, 2020–2033. doi:10.1093/brain/awv112.

Vogel, J.W., Iturria-Medina, Y., Strandberg, O.T., Smith, R., Levitis, E., Evans, A.C., Hansson, O., 2020. Spread of pathological tau proteins through communicating neurons in human Alzheimer's disease. Nat. Commun. 11, 2612. doi:10.1038/s41467-020-15701-2.

Xia, W., Zhang, B., Yang, Y., Wang, P., Yang, Y., Wang, S., 2015. Poorly controlled cholesterol is associated with cognitive impairment in T2DM: a resting-state fMRI study. Lipids Health Dis 14, 47. doi:10.1186/s12944-015-0046-x.

Yang, S., Wu, M., Ajilore, O., Lamar, M., Kumar, A., 2016. Metabolic aberrations impact biophysical integrity of macromolecular protein pools in the default mode network. Diabetes 65, 3464–3472. doi:10.2337/db15-1714.

Yi, L., Wang, J., Jia, L., Zhao, Z., Lu, J., Li, K., Jia, J., He, Y., Jiang, C., Han, Y., 2012. Structural and functional changes in subcortical vascular mild cognitive impairment: a combined voxel-based morphometry and resting-state fMRI study. PLoS One 7, e44758. doi:10.1371/journal.pone.0044758.

Zhang, T., Li, H., Zhang, J., Li, X., Qi, D., Wang, N., Zhang, Z., 2016. Impacts of high serum total cholesterol level on brain functional connectivity in non-demented elderly. J. Alzheimers Dis. 50, 455–463. doi:10.3233/JAD-150810.

Zlokovic, B.V., 2011. Neurovascular pathways to neurodegeneration in Alzheimer's disease and other disorders. Nat. Rev. Neurosci. 12, 723–738. doi:10.1038/nrn3114.

Zonneveld, H.I., Pruim, R.H., Bos, D., Vrooman, H.A., Muetzel, R.L., Hofman, A., Rombouts, S.A., van der Lugt, A., Niessen, W.J., Ikram, M.A., Vernooij, M.W., 2019. Patterns of functional connectivity in an aging population: The Rotterdam Study. Neuroimage 189, 432–444. doi:10.1016/j.neuroimage.2019.01.041.